47

The Boron Fullerenes

Arta Sadrzadeh
Rice University

Boris I. Yakobson
Rice University

47.1 Introduction

There are three phases for the bulk boron: α- rhombohedral, β-rhombohedral [1,2], and α-tetragonal [3]. α-Rhombohedral is made of B_{12} units, with lattice constant 5.30 Å and angle 58.13° [4] (Figure 47.1). Each B_{12} icosahedron is slightly distorted due to the Jahn–Teller effect, reducing the symmetry from I_h to D_{3d} [4]. β-Rhombohedral has a somewhat complicated unit cell, composed of 105 atoms, with lattice constant 10.15 Å and angle 65.17° [2,5]. A striking B_{84} structure with icosahedral symmetry can be identified in β-rhombohedral [6]. α-Tetragonal unit cell is made of 50 atoms, with lattice constants $a = 8.75$ Å and $c = 5.06$ Å [4]. It contains four B_{12} icosahedral and two isolated 4-bonded atoms. Recently, by means of *ab initio* studies, it has been shown that α-rhombohedral is more stable than β-rhombohedral [7]. α-Rhombohedral bulk is a semiconducting material with an energy gap of ~2 eV [4].

Systematic experimental and theoretical work on noncrystalline boron started in the 1980s. Mass spectra of boron clusters were obtained in a series of experimental studies performed by Hanley et al. [8,9]. Further important experimental study on the mass spectra was performed by La Placa et al. [10]. The method used was laser ablation of hexagonal boron nitride, and the mass of the clusters was separated by a time-of-flight technique. The experimental data showed "magic numbers" by boron cations of the size of 5, 7, 10, and 11.

Based on a series of *ab initio* simulations, Boustani proposed an "Aufbau Principle," stating that the most stable boron clusters can be constructed using two basic units: pentagonal and hexagonal pyramids, B_6 and B_7, respectively [11].

The boron clusters up to the size of 20 atoms have been shown to fall into two major categories: quasi-planar and compact. Figure 47.2 shows different isomers with 14 or fewer atoms [12].

Kiran et al. showed that planar-to-tubular structural transition occurs at B_{20} [13]. Further theoretical studies led by Boustani showed that indeed tubular structures (more precisely, double ring structures) are energetically favorable for larger clusters [14–16].

The aromaticity of small boron clusters has been studied by Zhai et al. [17]. It is shown that aromatic (planar) boron clusters possess more circular shapes, whereas anti-aromatic ones are elongated.

47.2 Boron Fullerenes

The existence of pure boron fullerenes was predicted recently [18]. The main idea is reinforcing hexagonal facets of boron isomorphs of carbon fullerenes by adding a boron atom at each center. Even though there is no direct experimental evidence for these fullerenes, their unusual stability and chemistry are interesting. Theoretical investigation in this direction is appealing since carbon fullerenes also went undetected for years, after their theoretical prediction in the early 1970s [19,20].

The most stable out of all boron fullerenes studied is the so-called boron buckyball, B_{80} (Figure 47.3b). The molecule is energetically favorable and symmetrically almost icosahedral (see Section 47.5). It has characteristics similar to B_{12}, which is the building block of all bulk phases, in the sense that it is made from crossing double rings (DRs). In Figure 47.3 (right), this similarity is highlighted. Figure 47.3b shows two crossing B_{30} DRs that are constituents of the cage. The whole cage is made up of three such pairs (six DRs in total). The staggered configuration

47-1

FIGURE 47.1 The lattice structure of α-rhombohedral bulk boron. Each atom is covalently bonded to five intra-icosahedral, and one or two inter-icosahedral atoms. (From Quandt, A. and Boustani, I., *ChemPhysChem*, 6, 2001, 2005. With permission.)

of each DR is formed by two rings, each containing 15 atoms and rotated by $\pi/15$ with respect to the one another.

Other members of boron fullerene family, obtained similarly, can also be considered. We limit the case to all possible cages with a size of 80 atoms or fewer (derived from fullerenes with less than 60 atoms before hexagonal reinforcement), as well as one bigger cage, B_{110}. Before reinforcement, the cages are boron isomorphs of C_{24}, C_{26}, C_{28}, C_{32}, C_{36}, C_{50}, and C_{80} fullerenes (specified by D_6, D_{3h}, D_3, D_3, D_{6h}, D_{5h}, and I_h symmetries, respectively). After the reinforcement, optimization shows that only four of these cages, shown in Figure 47.4a, sustain the hollow structure [18].

We can also consider cages B_{72} and B_{92}, formed by placing extra boron atoms on top of pentagons (B_{72}) and on pentagons and hexagons (B_{92}) of the B_{60}. Optimized structures are shown in Figure 47.4b. The B_{72} cage is round and preserves I_h symmetry but is less stable than B_{80}. The B_{92} is completely built from triangular bonding units, which are generally favorable for boron clusters [17]. However, this cage is also less stable than the B_{80} cage.

None of these structures consist of DRs, and perhaps for this reason, they do not have the exceptional stability as B_{80}. Table 47.1 summarizes the symmetries, values of cohesive energy (E_{coh}), and

FIGURE 47.2 Structure and symmetry of boron clusters with 14 atoms or fewer. (From Quandt, A. and Boustani, I., *ChemPhysChem*, 6, 2001, 2005. With permission.)

FIGURE 47.3 (a) B_{12} and (b) B_{80} clusters; they can both be seen as six interwoven double rings. (From Szwacki, N.G. et al., *Phys. Rev. Lett.*, 98, 166804, 2007. With permission.)
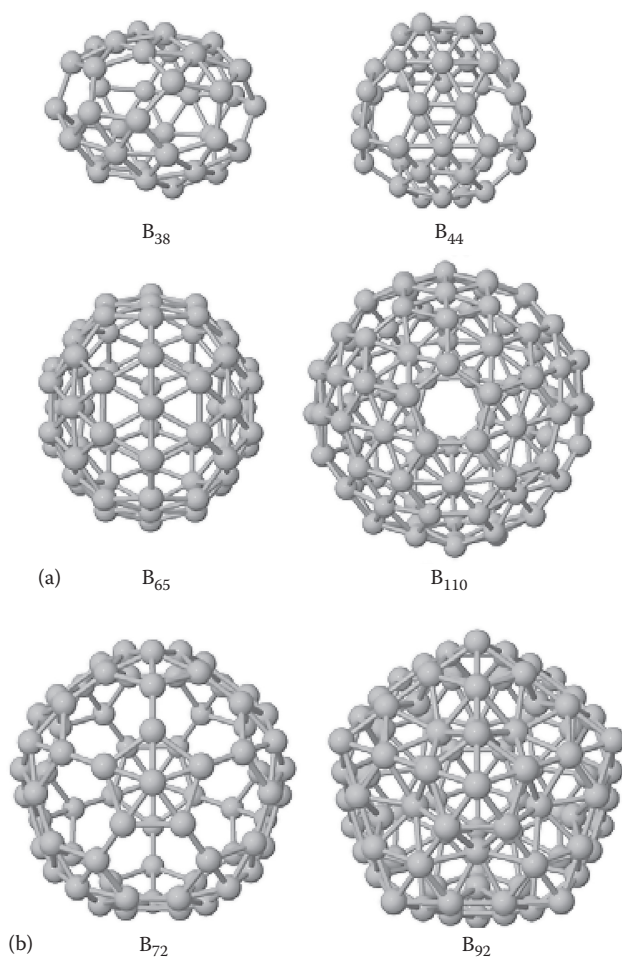
FIGURE 47.4 (a) Four other members of boron fullerene family. (b) B_{72} and B_{92}, which are formed by placing additional boron atoms at the center of pentagons of B_{60} and B_{80}. (From Szwacki, N.G. et al., *Phys. Rev. Lett.*, 98, 166804, 2007. With permission.)

TABLE 47.1 Symmetry, Cohesive Energy, and HOMO–LUMO Gaps of the Structures Considered Here

	Symmetry	E_{coh} (eV/atom)	HOMO–LUMO (eV)
B_{12}	I_h	5.01 (5.00)	0.737 (0.810)
B_{20}	I_h	4.74 (4.69)	1.253 (0.008)
B_{38}	D_3, distorted	5.47 (5.48)	0.935 (0.923)
B_{44}	D_{2h}, distorted	5.55 (5.56)	0.980 (0.965)
B_{60}	I_h	4.93 (4.91)	0.049 (0.050)
B_{65}	D_{5h}	5.69 (5.70)	0.095 (0.014)
B_{72}	I_h	5.60 (5.58)	0.269 (0.001)
B_{80}	I_h	5.76 (5.77)	1.006 (0.993)
B_{92}	I_h	5.72 (5.75)	1.129 (1.161)
B_{110}	I_h	5.73 (5.74)	0.119 (0.097)

Source: Szwacki, N.G. et al., *Phys. Rev. Lett.*, 98, 166804, 2007. With permission.

highest occupied-lowest unoccupied molecular orbital energy gap (HOMO–LUMO) of the above structures. In the case of B_{80}, there are 60 longer (l_{ph} = 1.73 Å) and 30 shorter (l_{hh} = 1.68 Å) bonds, making the diameter of B_{80} close to d = 8.17 Å (compared to corresponding value for C_{60}; d = 6.83 Å).

Recent calculations show that DR B_n clusters with n = 20, 24, 32, and 36 are the most stable structures among all clusters with the same number of atoms [13–16,21]. Taking DRs as reference point, the comparison between cohesive energies of the above structures and DRs is illustrated in Figure 47.5. "Strip" in the figure corresponds to infinite DR.
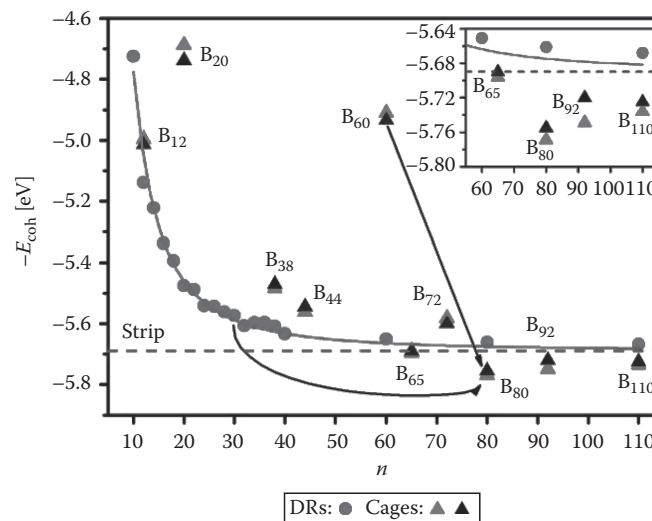
FIGURE 47.5 Cohesive energy per atom as a function of the number of atoms "n" in the B_n clusters. The circles correspond to double rings, whereas the black (magenta) triangles correspond to cages calculated with Quantum-ESPRESSO (GAUSSIAN03). The gray horizontal line corresponds to the cohesive energy of the infinite double-ring (strip). The arrows show the increase in cohesive energy by reinforcement of hexagons (from B_{60} to B_{80}) and by appropriate crossing of the double rings to form the icosahedral structure (from B_{30} DR to B_{80}). The inset shows relative E_{coh} values for four cages B_{65}, B_{80}, B_{92}, and B_{110}, more pronouncedly. (From Szwacki, N.G. et al., *Phys. Rev. Lett.*, 98, 166804, 2007. With permission.)

(a)

(b)
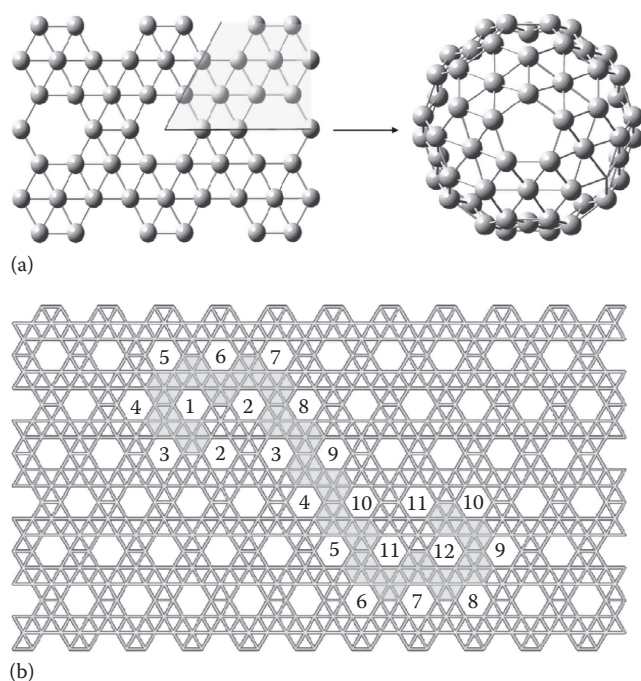
FIGURE 47.6 (a) Atoms in shaded area of the α-sheet (left) are removed, and the ones on the lines are identified to form pentagonal disclination in B_{80} (right). Figure shows only half of the molecule. (b) Projection of B_{80} on α-sheet. Numbered facets represent the pentagons in B_{80}. (From Sadrzadeh, A. et al., *J. Phys. Chem. A*, 112, 13679, 2008. With permission)

47.3 Boron Sheet

B_{80} (like C_{60}) can be imagined as a sheet wrapped on sphere. The most stable structure for the sheet, the α-sheet, was recently reported [22]. The special pattern as a honeycomb lattice wherein 2/3 of the hexagonal centers are filled ensures the best occupancy of the bands by electrons and therefore lowest energy (Figure 47.6). Upon wrapping the α-sheet on a sphere, "empty" hexagons are replaced by 12 pentagonal disclinations required topologically, and strips enclosing them are replaced by B_{30} DRs. Figure 47.6a shows how the sheet can be folded to form a pentagonal disclination. Figure 47.6b highlights the unfolded B_{80} molecule on an α-sheet.

The bond length in α-sheet is 1.70 Å, and its cohesive energy (obtained by the same method used for values in Table 47.1) is 5.93 eV/atom. The α-sheet is metallic, with zero energy gap between the bands.

47.4 Boron Nanotubes

Fullerenes can be viewed as short nanotubes. Here we briefly describe physical properties of boron nanotubes (BTs).

BTs can be obtained by wrapping the sheet along the chiral vector. Since α-sheet is believed to be the most stable pattern for the sheet, we only describe α-BTs. We choose the indexing of the BTs to correspond to the long-accepted convention for the CNTs— with the two $\sqrt{3} \cdot b$-long (where b is the bond length) basis vectors 60° apart, each directed along the zigzag motif in the lattice. The tube circumference is specified as a pair of components (n, m). This implies that any (n, m) tube derived from α-sheet exists only when (n–m) is a multiple of three [23].

In contrast to CNTs, BTs are metallic or semiconducting depending on their diameter alone. For diameters smaller than 1.7 nm, BTs are semiconducting [24]. Figure 47.7 shows dependence of the band gap on the diameter for armchair BT [23]. Zigzag tubes have a close value of transition from metallic to semiconducting diameter. One can attribute semiconducting behavior of the BTs to their relaxation, which causes central B atoms buckling inward, thus opening the band gap.

(a)

(b)

(c)
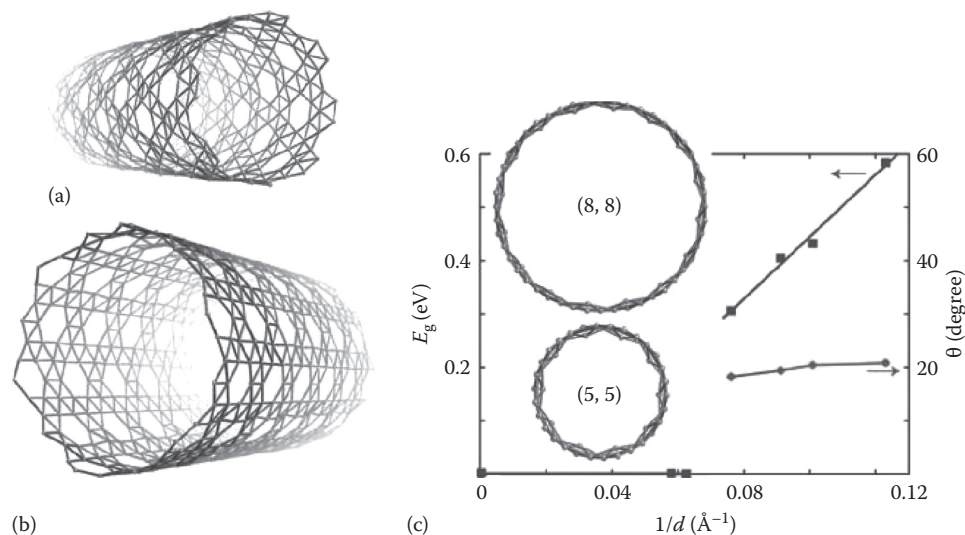
AQ2   **FIGURE 47.7** (a) An armchair and (b) a zigzag α-boron nanotube. (c) Dependence of the band gap (blue line) and dihedral angle of the off-plane atoms with respect to six-membered ring (red line) on inverse of diameter. Inset shows how relaxation causes buckling in two cases of (5, 5) and (8, 8) α-BT. (From Singh, A.K. et al., *Nano Lett.*, 8, 1314, 2008. With permission.)

FIGURE 47.8 High resolution TEM image of B-nanotubes of ~3 nm diameter, grown on silica template (picture from Prof. L. Pfefferle's site, Yale University, and similar to Fig. 1 in [25]). (From Ciuparu, D. et al., *J. Phys. Chem. B*, 108, 3967, 2004. With permission.)

Radial breathing mode (RBM) frequency dependence on the diameter can be obtained from parameters describing shell mechanical properties (in-plane stiffness and Poisson ratio), which can be estimated by $f_{RBM} \cong 210 \, nm/d$, cm^{-1} [23].

Single-wall BTs with diameter 3 nm have been synthesized by Ciuparu et al. [25] (Figure 47.8). The reported Raman breathing mode peak is at frequency 210 cm^{-1}, which is at odds with theoretical value (~70 cm^{-1}). The peak might be due to the presence of other boron structures in the samples (B$_{80}$ for instance).

47.5 Isomerization

There are various isomers of boron buckyball that are close to each other in energy and structure [26]. Here we consider three B$_{80}$ isomers obtained by B3LYP/6-31G(d) structural optimization [27]. Visually, their geometries are almost identical; however, a detailed analysis reveals important differences in their symmetries [26,28]. Namely, two out of three structures under consideration are very close to having icosahedral (I$_h$) and tetrahedral (T$_h$) [29] symmetries, while the third one appears to have no symmetry at all (C$_l$). Correspondingly, we denote these B$_{80}$ isomers as I$_h$, T$_h$, and C$_l$. All the optimizations were performed without any symmetry restrictions. Therefore, they correspond to true local minima of potential energy surface. The I$_h$ isomer lies lowest in energy, with total energy 3.6 meV lower than T$_h$ one and 30.3 meV lower than C$_l$ one (the total

energy differences are clearly very small and are sensitive to the method) [26].

To estimate the deviations of I$_h$ and T$_h$ isomers from the corresponding ideal symmetries, let us consider the values of the dihedral angle between the six-membered ring and the plane formed by two of its atoms and the central boron atom. For the I$_h$ isomer, the dihedral angles are from 3.26° to 3.81° (toward the center of the buckyball), that is, their deviation from the average is negligible (less than 0.3°). In the case of the T$_h$ structure, there is one group of eight central atoms with dihedral angles of 8.88° to 9.07° toward the center, and another group of 12 central atoms with small (~1°) dihedral angles away from the center. T$_h$ isomer is similar to the "isomer A" of Ref. [29]. For comparison, the dihedral angles in the C$_l$ isomer vary from 7.54° toward the buckyball center to 1° away from it.

The symmetry is more visibly reflected in electron charge transfer from central boron atoms to the B$_{60}$ skeleton [28]. The amount of Mulliken charge transfer is 0.149e to 0.154e in I$_h$ case, 0.063e to 0.065e for the group of 8 atoms, 0.232e to 0.233e for the group of 12 atoms in T$_h$ case, and in the range of 0.074e to 0.205e in C$_l$ case (Figure 47.9).

The symmetry of the B$_{80}$ isomers under consideration can be further confirmed by the analysis of their electronic structure, as follows.

47.6 Electronic Structure

There are 200 occupied MOs in B$_{80}$. It is helpful to think of them as linear combinations of the boron atomic orbitals (AOs) and to distinguish between the AOs belonging to the two nonequivalent groups of boron atoms, namely, the 20 atoms situated in the centers of hexagons and the 60 others forming a structure analogous to C$_{60}$ [26].

The lowest 80 MOs are linear combinations of 1s-AOs of boron atoms, with a negligible contribution of higher AOs. The 20 boron atoms in the centers of hexagons mainly contribute to the MOs 1–20, which have very close energies; the other 60 atoms contribute to the MOs 21–80, which are also nearly degenerate.

C$_l$ T$_h$ I$_h$
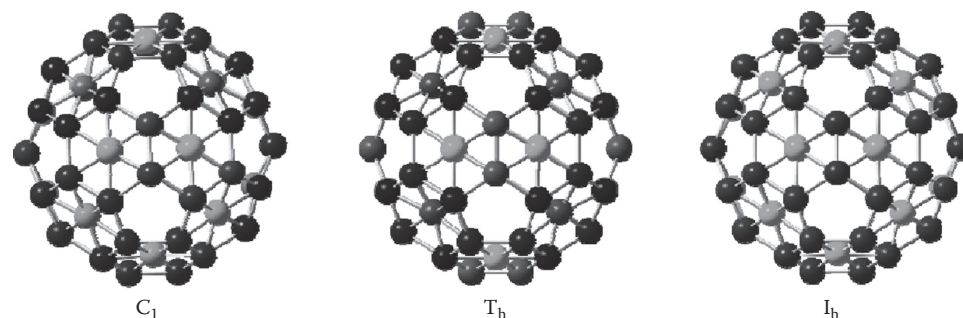
AQ3   **FIGURE 47.9** Mulliken charges are shown for the three isomers C$_l$, T$_h$, and I$_h$. Green (red) corresponds to positive (negative) atomic charges. The brighter green corresponds to more positive charge and smaller dihedral angle. (From Szwacki, N.G. et al., *Phys. Rev. Lett.*, 100, 159901, 2008. With permission.)
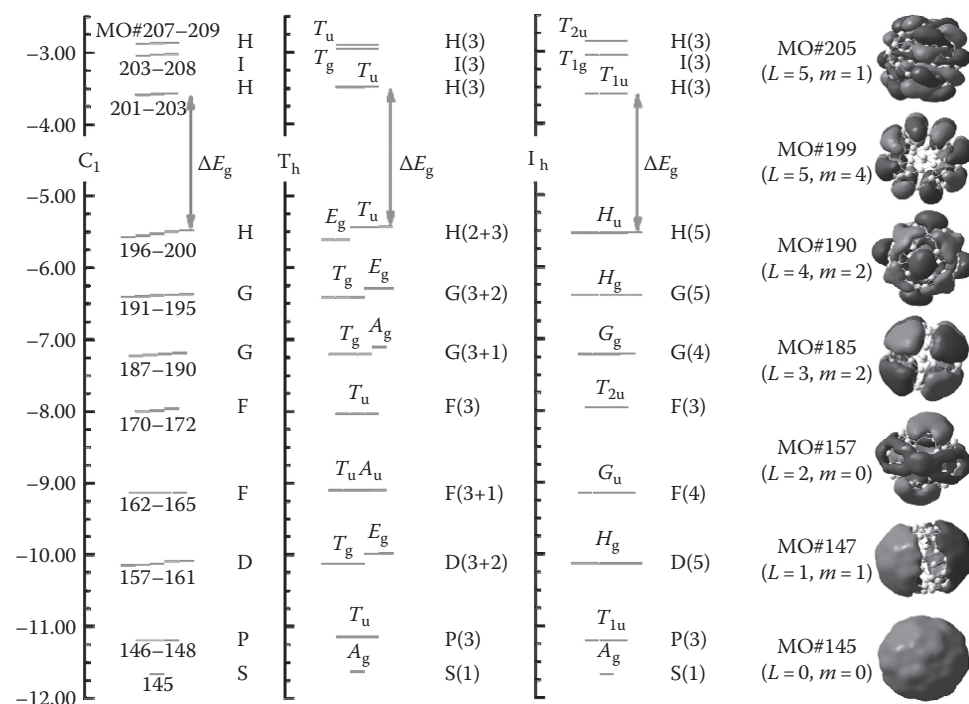
FIGURE 47.10 Energy diagram showing the π-type molecular orbitals of different isomers of B_{80}, calculated with B3LYP/6-31G(d) method/basis. The left, middle, and right diagrams correspond to C_1, T_h, and I_h isomers, respectively. The levels with energy difference less than 10 meV are considered degenerate. The green arrow marks the HOMO–LUMO gap (ΔE_g = 1.88, 1.95, 1.93 eV for C_1, T_h, and I_h, respectively). For the energy levels of T_h and I_h structures, the corresponding representations are shown. For each type of spherical harmonics (S, P, D, etc.), the spatial distribution of one typical molecular orbital is shown in the right column. (From Sadrzadeh, A. et al., *J. Phys. Chem. A*, 112, 13679, 2008. With permission.)

The higher occupied MOs of B_{80} are mostly made of boron 2s- and 2p-AOs and can have either σ or π character. There are only 60 π-electrons in the structure (which can be thought of as donated by the sixty equivalent boron atoms), and correspondingly, 30 π-orbitals are occupied.

Molecular orbitals of a nearly spherical molecule can be well approximated by the spherical harmonics [30,31], and thus strongly resemble AOs of various types. The MOs that have the azimuthal quantum number L = 0, 1, 2, 3, 4, 5, 6, etc., are commonly designated as S, P, D, F, G, H, I, etc. orbitals, analogous to the standard AO naming.

As the frontier molecular orbitals of B_{80} are of π-type, we concentrate on the π-MOs. Their energies for three isomers with C_1, T_h, and I_h symmetries are shown in Figure 47.10. One may compare this energy diagram with that of C_{60} [30]. Notice that the numbers of occupied π-orbitals in both C_{60} and B_{80} equal 30 and thus do not satisfy the $2(N + 1)^2$ Hirsch aromaticity rule [32], because the H shell (L = 5) is not filled completely.

The rightmost column in Figure 47.10 shows the spatial distribution of one typical molecular orbital for each quantum number L [33]. The orbital degeneracy is determined by the azimuthal quantum number L and the symmetry of the molecule under consideration. For example, the fivefold degenerate d-type atomic orbitals of transition metals split into a triplet

and a doublet in the octahedral crystal field (see e.g., Ref. [34]). Similarly, lowering the isomer symmetry from I_h to T_h leads to the orbital splitting, clear for instance for HOMO (MOs #196–200, H-type) in Figure 47.10. In particular, the symmetries of structures are reflected in their HOMO degeneracy: it is fivefold for I_h (within 5 meV), threefold for T_h (within 2 meV), and nondegenerate for C_1. For the two symmetrical isomers, T_h and I_h, the representations of their symmetry groups are shown for all the π-type molecular orbitals in Figure 47.10.

Since the symmetric (I_h) structure has a nondegenerate ground state (HOMO is fully filled), symmetry breaking is not due to Jahn–Teller effect.

47.7 Vibrational Modes

To analyze the vibrational modes of boron buckyball, we use B3LYP/STO-3G method/basis [27] because of the computational burden (for a more detailed analysis of vibrational modes, see [35]). The B_{80} geometry used for this analysis was relaxed using the same method, and has T_h symmetry. It is close to "isomer B" of Ref. [29], with 12 (8) central atoms making dihedral angle ~12.5° (8°) toward (away from) the center. B_{80} has 64 distinct intramolecular mode frequencies ranging from 154 cm⁻¹ for radial vibrations to 1181 cm⁻¹ for tangential ones. The low lying frequencies correspond to the central atom vibrations.

The breathing mode frequency is 474 cm⁻¹. In this mode, the 12 central hexagonal atoms with dihedral angle toward the center move in opposite phase with respect to the rest of the atoms. It is worth noting that in the Raman spectrum reported for BT samples [25], there is a peak close to this value of frequency (~420 cm⁻¹). The authors of Ref. [25] attribute the peaks at the range of 400–600 cm⁻¹ to either smaller diameter BT or t"other boron structures present in the sample."

47.8 Other Boron Fullerenes

Recently, there was a report on a new family of boron fullerenes, with the number of atoms $32 + 8k$ [36]. A subfamily with the number of atoms $80 + 8k$ are obtained by modified leapfrog transformation (MLT), from C_{20+2k} (Figure 47.11). In MLT, one starts with C_{20+2k}, fill all the facets, make the Wigner–Seitz dual, and then fill the hexagons except for the ones that fall inside the original hexagons of C_{2k+2}.

The symmetries, cohesive energies, and HOMO–LUMO gaps are summarized in Table 47.2. In the limit of $k = 0$ and ∞, one obtains B_{80} and α-sheet, respectively. The authors of Ref. [36] propose an isolated hollow rule as well as a counting rule for electrons. Counting is explained simply as two electrons shared in each triangular (three-center) bond. In B_{80}, there are 20 hexagons and 120 triangles, hence, 240 valence electrons. In the α-sheet, there are 12 triangles in the unit cell and, correspondingly, 24 valence electrons (there are 8 atoms in α-sheet unit cell).

Recently, B_{12} stuffed fullerene-like boron clusters were studied, and it was shown that B_{98-102} clusters are thermodynamically more stable than B_{80} [37]. Also, there was a report on other fullerenes composed of six double rings, with comparable stability to B_{80} [38].

47.9 Applications

Such structures should have a wide variety of applications [39]. One possible application is in cancer therapy. Boron in nature consists of the isotopes ^{10}B (19.6%) and ^{11}B (80.4%). The ^{10}B isotope has a special property that has long been exploited in nuclear reactors, namely, it has very high neutron absorption cross section (3835 barns) [40]. The reaction of ^{10}B with thermal neutron generates ^{7}Li and α particles, with latter having energies that make them lethal to nearby cell [40]. This aspect alone makes search for boron clusters of different shape, size, and cell-penetration ability very important. Another important and recently discussed possibility is in use of boron (with proper addition of metal atoms) clusters for efficient hydrogen storage [41].

Rotary motion along a molecular axis, controllable by a single electron transfer or photoexcitation, has been proposed for metallacarboranes (Figure 47.12) [42]. The existence of this or possibly other boron-derived molecular motors has been sought for many years, as a parallel to biological motors that can be powered by light or electrical energy, rather than ATP.

AQ4
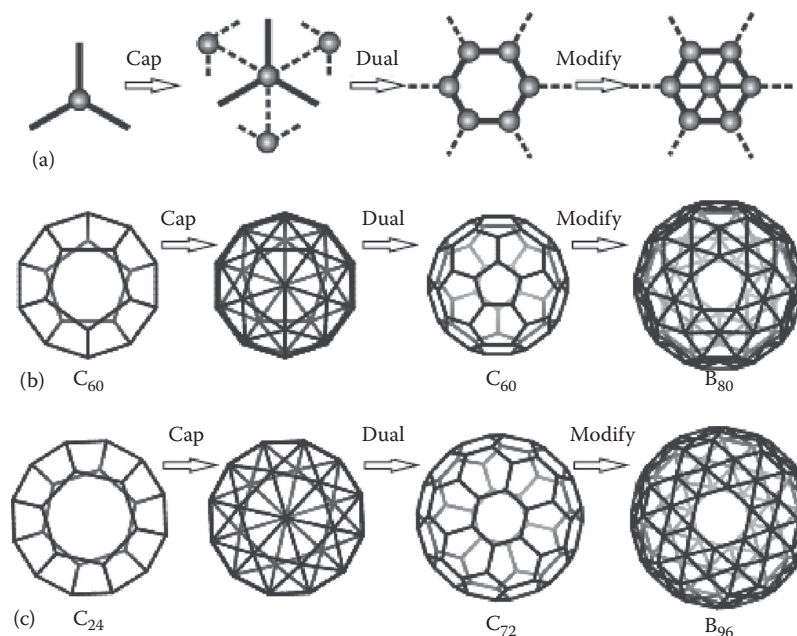
FIGURE 47.11 Illustration of leapfrog and modified leapfrog transformations. (a) A three-connected vertex becomes a new hexagon (in leapfrog) or a hexagon with an additional atom in center (in modified leapfrog); (b) a C_{20} converts to C_{60} and B_{80} by the leapfrog and modified leapfrog transformations, respectively; (c) a C_{24} transforms to C_{72} and B_{96}. (From Q.-B. Yan et al., *Phys. Rev. B*, 78, 201401, 2008. With permission.)

TABLE 47.2 The Number (N_{iso}), Symmetries, Energies per Atom (E, in eV) Relative to That of Graphene and α-Sheet, Respectively, and HOMO–LUMO Gap Energies (ΔE, in eV) of C_{60+6k} and B_{80+8k} Fullerenes ($k \le 5$) Obtained with PBEPBE/6-31G Method/Basis

k	N_{iso}	Symmetry	$C_{n=60+6k}$			$B_{n=80+8k}$				
			n	E	ΔE	n	E	ΔE	N_{HH}	N_{FH}
0	1	I_h	60	0.386	1.670	80	0.179	1.020	0	20
1	0									
2	1	D_{6d}	72	0.365	1.445	96	0.160	0.784	3	24
3	1	D_{3h}	78	0.346	1.460	104	0.151	0.738	4	26
4	2	D_2	84	0.339	1.367	112	0.146	0.682	5	28
		T_d	84	0.329	1.632	112	0.141	0.927	5	28
5	3	C_{2v}^1	90	0.321	1.364	120	0.137	0.709	6	30
		C_{2v}^{11}	90	0.322	1.489	120	0.136	0.828	6	30
		D_{5h}	90	0.312	1.029	120	0.135	0.555	6	30

Source: Yan, Q.-B. et al., *Phys. Rev.* B, 78, 201401, 2008. With permission.

Note: The authors believe that N_{HH} should be simply equal to k; however, we present the original reported Table I in [36].
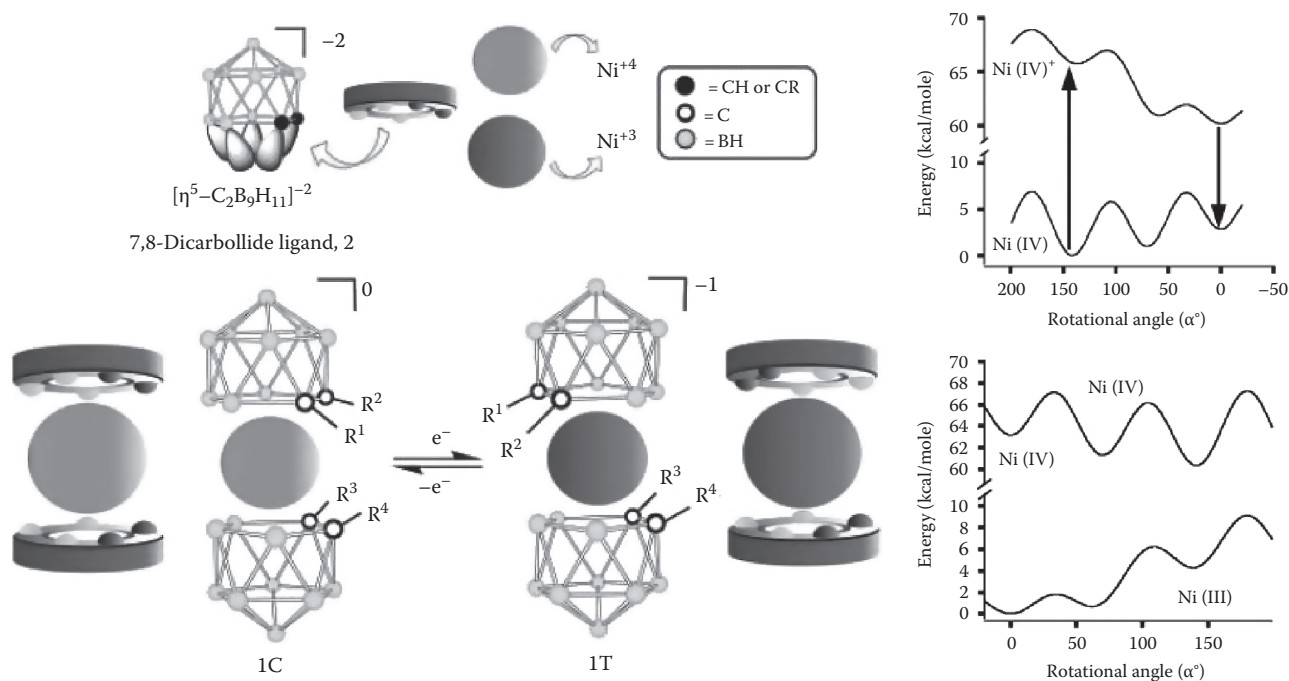
FIGURE 47.12 (Left) Illustration of rotor configurations of Ni(IV) (1C) and Ni(III) (1T) and the structural modules from which they are constructed. Structure 1T is defined with rotation angle 0°. R^1, R^2, R^3, and R^4 represent H here. (Right) Calculated energy of the ground and excited electronic state of the neutral Ni(IV) configuration as a function of rotation angle. (Reassembled from M.F. Hawthorne et al., *Science*, 303, 1849, 2004. With permission.)

47.10 Summary

This chapter discusses the physical properties of pure boron fullerenes, sheets, and nanotubes, as well as the bulk. There are three phases for the bulk boron: α- and β-rhombohedral [1,2], and α-tetragonal [3]. The most stable structure for the sheet is the so-called α-sheet, which was recently reported by Tang and Ismail-Beigi [22].

Wrapping α-sheet around a cylinder generates different (zigzag and armchair) α-boron tubes (α-BT) [23,24]. It turns out that for diameters smaller than 1.7 nm, BTs are semiconducting. Single-wall BTs with a diameter of 3 nm have been synthesized by Ciuparu et al. [25].

The boron buckyball, B_{80}, was reported recently as boron isomorph of C_{60}, with all the 20 hexagons reinforced by extra atoms [18,28]. The boron buckyball can also be understood as

the α-sheet wrapped around a sphere (Figure 47.6) [26]. The electronic structure and vibrational modes of different isomers of B_{80} are also discussed. We conclude the chapter by discussing a new family of boron fullerenes, with $(80 + 8k)$ atoms for which B_{80} is a special case [36], as well as possible applications of boron clusters.

References

1. B. F. Decker and J. S. Kasper, *Acta Crystallogr*. **12**, 503 (1959).
2. B. Callmer, *Acta Crystallogr., Sect. B: Struct. Crystallogr. Cryst. Chem*. **33**, 1951 (1977).
3. A. W. Laubengayer, D. T. Hurd, A. E. Newkirk, and J. L. Hoard, *J. Am. Chem. Soc*. **65**, 1924 (1943).
4. D. Li, Y.-N. Xu, and W. Y. Ching, *Phys. Rev. B* **45**, 5895 (1992).
5. J. L. Hoard, D. B. Sullenger, C. H. L. Kennard, and R. E. Hughes, *J. Solid State Chem*. **1**, 268 (1970).
6. E. D. Jemmis and D. L. V. K. Prasad, *J. Solid State Chem*. **179**, 2768 (2006).
7. A. Masago, K. Shirai, and H. Katayama-Yoshida, *Phys. Rev. B* **73**, 104102 (2006).
8. L. Hanley and S. L. Anderson, *J. Chem. Phys*. **89**, 2848 (1988).
9. L. Hanley, J. Whitten, and S. L. Anderson, *J. Phys. Chem*. **92**, 5803 (1988).
10. S. J. La Placa, P. A. Roland, and J. J. Wynne, *Chem. Phys. Lett*. **190**, 163 (1992).
11. I. Boustani, *Phys. Rev. B* **55**, 16426 (1997).
12. A. Quandt and I. Boustani, *ChemPhysChem* **6**, 2001 (2005).
13. B. Kiran, S. Bulusu, H.-J. Zhai, S. Yoo, X. C. Zeng, and L.-S. Wang, *Proc. Natl. Acad. Sci. U S A* **102**, 961 (2005).
14. I. Boustani and A. Quandt, *Europhys. Lett*. **39**, 527 (1997).
15. I. Boustani, A. Rubio, and J. Alonso, *Chem. Phys. Lett*. **311**, 21 (1999).
16. S. Chacko, D. G. Kanhere, and I. Boustani, *Phys. Rev. B* **68**, 035414 (2003).
17. H.-J. Zhai, B. Kiran, J. L. Li, and L.-S. Wang, *Nat. Mater*. **2**, 827 (2003).
18. N. G. Szwacki, A. Sadrzadeh, and B. I. Yakobson, *Phys. Rev. Lett*. **98**, 166804 (2007).
19. E. Osawa, *Kagaku* **25**, 854 (1970).
20. D. A. Bochvar and E. G. Gal'pern, *Proc. Acad. Sci. USSR* **209**, 610 (1973).
21. M. A. L. Marques and S. Botti, *J. Chem. Phys*. **123**, 014310 (2005).
22. H. Tang and S. Ismail-Beigi, *Phys. Rev. Lett*. **99**, 115501 (2007).
23. A. K. Singh, A. Sadrzadeh, and B. I. Yakobson, *Nano Lett*. **8**, 1314 (2008).
24. X. Yang, Y. Ding, and J. Ni, *Phys. Rev. B* **77**, 041402 (2008).
25. D. Ciuparu, R. F. Klie, Y. Zhu, and L. Pfefferle, *J. Phys. Chem. B* **108**, 3967 (2004).
26. A. Sadrzadeh, O. V. Pupysheva, A. K. Singh, and B. I. Yakobson, *J. Phys. Chem. A* **112**, 13679 (2008).
27. M. J. Frisch, G. W. Trucks, H. B. Schlegel, G. E. Scuseria, M. A. Robb et al., *Gaussian 03, Revision C.02* (Gaussian, Inc., Wallingford, CT, 2004).
28. N. G. Szwacki, A. Sadrzadeh, and B. I. Yakobson, *Phys. Rev. Lett*. **100**, 159901 (2008).
29. G. Gopakumar, M. T. Nguyen, and A. Ceulemans, *Chem. Phys. Lett*. **450**, 175 (2008).
30. Z. Chen and R. B. King, *Chem. Rev*. **105**, 3613 (2005).
31. W. A. de Heer, *Rev. Mod. Phys*. **65**, 611 (1993).
32. M. Buhl and A. Hirsch, *Chem. Rev*. **101**, 1153 (2001).
33. http://www.orbitals.com/orb/orbtable.htm.
34. I. B. Bersuker, *Electronic Structure and Properties of Transition Metal Compounds: Introduction to the Theory* (Wiley, New York, 1996).
35. T. Baruah, M. R. Pederson, and R. R. Zope, *Phys. Rev. B* **78**, 045408 (2008).
36. Q.-B. Yan, X.-L. Sheng, Q.-R. Zheng, L.-Z. Zhang, and G. Su, *Phys. Rev. B* **78**, 201401 (2008).
37. D. L. V. K. Prasad and E. D. Jemmis, *Phys. Rev. Lett*. **100**, 165504 (2008).
38. N. G. Szwacki, *Nano. Res. Lett*. **3**, 49 (2008).
39. R. N. Grimes, *J. Chem. Educ*. **81**, 657 (2004).
40. M. F. Hawthorne, *Pure Appl. Chem*. **63**, 327334 (1991).
41. Y. Zhao, M. T. Lusk, A. C. Dillon, M. J. Heben, and S. B. Zhang, *Nano Lett*. **8**, 157 (2008).
42. M. F. Hawthorne, J. I. Zink, J. M. Skelton, M. J. Bayer, C. Liu, E. Livshits, R. Baer et al., Science **303**, 1849 (2004).